EBioMedicine 65 (2021) 103251

Contents lists available at ScienceDirect

EBioMedicine

journal homepage: www.elsevier.com/locate/ebiom

Research paper

The role of LR-TIMAP/PP1c complex in the occurrence and development of no-reflow

Xiaoyu Quan[a,1], Xiucheng Liu[a,b,1], Xichun Qin[a,b,1], Yuzhuo Wang[b], Teng Sun[a,b], Zhimin Li[b], Lidong Zhu[b], Jiali Chen[b], Yeqing Zhou[b], Sandeep Singh[c], Hongyan Dong[d], Zhongming Zhang[b,**], Hao Zhang[a,b,*]

[a] Thoracic Surgery Laboratory, the First College of Clinical Medicine, Xuzhou Medical University, Xuzhou, Jiangsu 221006, China
[b] Department of Thoracic Surgery, Affiliated Hospital of Xuzhou Medical University, 99 West Huaihai Road, Xuzhou, Jiangsu 221006, China
[c] School of International Education, Xuzhou Medical University, 209 Tongshan Road, Xuzhou, Jiangsu 221004, China
[d] Morphological Research Experiment Center, Xuzhou Medical University, 209 Tongshan Road, Xuzhou, Jiangsu 221004, China

ARTICLE INFO

Article History:
Received 22 August 2020
Revised 1 February 2021
Accepted 3 February 2021
Available online xxx

Keywords:
No-reflow
Laminin receptor
Phosphorylation
LR-TIMAP/PP1c complex

ABSTRACT

Background: The presence of no-reflow can increase the risk of major adverse cardiac events and is widely regarded as an important sign of serious prognosis. Previous studies show that laminin receptor (LR) is closely related to the morphology and function of microvessels. However, whether LR is involved in the occurrence and development of no-reflow is still unknown.

Methods: In vivo, positron emission tomography (PET) perfusion imaging was performed to detect the effects of intramyocardial gene (LR-AAV and LR-siRNA-AAV) delivery treatment on the degree of no-reflow. In vitro, LC-MS/MS analysis was conducted to identify the LR phosphorylation sites of human cardiac microvascular endothelial cells (HCMECs) treated with oxygen-glucose deprivation (OGD) for 4 h. Western blot analyses were used to evaluate the phosphorylation levels of LR at residues Tyr47 (phospho-Tyr47-LR/pY47-LR) and Thr125 (phospho-Thr125-LR/pT125-LR) and their effects on the phosphorylation of VE-cadherin residue Ser665 (phospho-Ser665-VE-cad).

Findings: LR over-expression, LR^{T125A} (phosphonull) and LR^{Y47A} (phosphonull) treatments were found to reduce the level of phospho-Ser665-VE-cad, and subsequently maintain adherent junctions and endothelial barrier integrity in hypoxic environments. Mechanistically, TIMAP/PP1c can combine with LR on the cell membrane to form a novel LR-TIMAP/PP1c complex. The level of pY47-LR determined the stability of LR-TIMAP/PP1c complex. The binding of TIMAP/PP1c on LR activated the protein phosphatase activity of PP1c and regulated the level of pT125-LR.

Interpretation: This study demonstrates that low level of phospho-LR reduces no-reflow area through stabilizing the LR-TIMAP/PP1c complex and promoting the stability of adherens junctions, and may help identify new therapeutic targets for the treatment of no-reflow.

1. Introduction

Disruption of endothelial barrier integrity, embolization and the subsequent no-reflow (NR) are closely related to the severity and prognosis of acute myocardial infarction (AMI) [1-3]. Recently, the American Heart Association concurred that the strategy of minimizing microvascular injury during AMI to benefit patients is well-established and should be prioritized for AMI management [4,5]. Consequently, studies focused on protection of endothelial barrier will re-energize development of effective therapies targeting AMI and no-reflow.

In most vascular beds, adherens junctions (AJs) are the major determinant of endothelial barrier integrity [6-9]. Vascular endothelial-cadherin (VE-cadherin), a specific component of AJs, has been reported to play a critical role in the contact and communication between endothelial cells [10,11]. VE-cadherin adhesion is mainly regulated by phosphorylation and dephosphorylation of its residues [12]. Hypoxia-induced phosphorylation of VE-cadherin residue Ser665 (phospho-Ser665-VE-cad) dramatically leads to the collapse of AJs and subsequent vascular dysfunction. This process involves a laminin receptor (LR)-dependent phosphorylation cascade signaling pathway, while the detailed molecular mechanism is yet to be established.

* Corresponding authors.
** Co-Corresponding authors.
E-mail address: zhanghao@xzhmu.edu.cn (H. Zhang), zhang_zhongming@xzhmu.edu.cn (Z. Zhang).
[1] These authors contributed equally to this work.

https://doi.org/10.1016/j.ebiom.2021.103251

Research in Context

Evidence before this study

The phenomenon of no-reflow seriously limits the therapeutic value of coronary recanalization and leads to poor prognosis. Generally, minimizing microvascular damage and maintaining endothelial barrier before coronary recanalization are believed to be critical to prevent no-reflow.

Laminin receptor (LR) is strongly expressed in endothelial cells (ECs) and is reported to play a vital role in inducing cell apoptosis and inhibiting cell migration. Hypoxia-induced phosphorylation of VE-cadherin residue Ser665 dramatically leads to the collapse of adherens junctions (AJs) and subsequent vascular dysfunction. This process involves a LR-dependent phosphorylation cascade signaling pathway, while the detailed molecular mechanism is yet to be established.

Our preliminary evidence showed a significant upregulation of phospho-LR in hypoxia-treated ECs and LR over-expression treatment could relieve the reduction of tissue perfusion and no-reflow, suggesting LR may be a new therapeutic targets for the treatment of no-reflow.

Added value of this study

Here, our study indicated that LR is closely related to the occurrence and severity of no-reflow. In vivo, LR over-expression or down-regulating the levels of phospho-Thr125-LR and phospho-Tyr47-LR could effectively protect the integrity of the endothelial barrier and reduce the no-reflow area. Mechanistically, we introduced a novel LR-TIMAP/PP1c complex in vitro, which is a crucial regulator of the level of phospho-LR and the stability of AJs.

Implications of all the available evidence

Our evidence introduced a crucial role of LR in maintaining microvascular AJs and vascular structural integrity through stabilizing the LR-TIMAP/PP1c complex. This important activity of LR or phospho-LR presents a novel therapeutic approach to manage and prevent no-reflow events after coronary recanalization so as to enhance functional recovery post revascularization therapy.

The 37/67-kd LR is closely involved in many pathological processes. As an extracellular matrix molecule, LR plays an important role in tumor cell migration, invasion, and angiogenesis [13,14]. In addition, LR is strongly expressed in endothelial cells and is reported to play a vital role in inducing cell apoptosis and inhibiting cell migration [15,16]. Studies also indicated that LR phosphorylation involves multiple biological processes, such as the formation of endothelial filopodia and the stability of microvessels [17]. Therefore, from a theoretical and empirical perspective, research into the role of LR in pathological no-reflow and the mechanism involved are meaningful.

Phospho-Ser/Thr-specific protein phosphatase 1 (PP1) consists of a catalytic subunit such as PP1cα, PP1cβ, and PP1cγ and a regulatory subunit such as the myosin phosphatase targeting protein (MYPT) family [18]. The regulatory subunit can control enzymatic activity by targeting holoenzyme to specific subcellular locations and substrates. TGF-β inhibited membrane associated protein (TIMAP), a member of the myosin MYPT family, is a positive regulator of endothelial barrier [19,20]. TIMAP contains a CAAX motif at the carboxyl terminus; prenylation of CAAX box proteins influences the subcellular localization of PP1 [21-23]. Kwanghee Kim and coworkers demonstrated that TIMAP targeted PP1c to dephosphorylate LR [24]. Therefore, we speculate that TIMAP/PP1c is involved in the regulation of phospho-Ser665-VE-cad and endothelial barrier integrity by LR.

The purposes of this study are: 1) to explore the role for LR in AMI and no-reflow; 2) to address whether the phosphorylation of LR down-regulates phospho-Ser665-VE-cad to protect endothelial barrier; 3) and to decipher related mechanism for this stimulation.

2. Methods

2.1. Reagents

Antibodies against vascular endothelial-cadherin (VE-cadherin; catalog #ab33168; 1:300, RRID: AB_870662), CD31 (catalog #ab24590; 1:200, RRID: AB_448167), 67 kDa Laminin Receptor (LR; catalog #ab133645; 1:100 for Co-IP, RRID: AB_2877125) and β-actin (catalog #ab54724; 1:1000, RRID: AB_940113) were obtained from Abcam (Cambridge, UK). Antibody of TIMAP (PPP1R16B; catalog #ap17590c; 1:1000 for WB, 1:100 for Co-IP and 1:50 for ICC/IF) was bought from Abgent (San Diego, USA). Antibody for PP1cβ (catalog #*Sc*-7482; 1:1000 for WB, 1:100 for Co-IP and 1:50 for ICC/IF, RRID: AB_628177) was purchased from Santa Cruz Biotechnology (Dallas, USA). Antibody of Lamin A/C (catalog #10298-1-ap; 1:1000, RRID: AB_2296961) was obtained from ProteinTech Group (Rosemont, USA). Antibodies for phospho-Ser43-LR (pS43-LR) (catalog #WG00412P), phospho-Tyr47-LR (pY47-LR) (catalog #WG00521P), phospho-Ser-75-78-79-LR (pS75-78-79-LR) (catalog #WG00617P) and phospho-Thr125-LR (pT125-LR) (catalog #WG00317P) were prepared from ABclonal (Boston, USA). Antibody for phospho-Ser665 VE-cadherin was prepared from Abgent (San Diego, USA). And LR/Alexa Fluor 350 Conjugated antibody (catalog #bs-0901R-AF350; 1:50) was bought from Bioss (Beijing, China). Secondary antibodies including Alexa Fluor 594 donkey anti-rabbit immunoglobulin G (catalog #A21207; 1:200, RRID: AB_141637) and Alexa Fluor 488 goat anti-mouse immunoglobulin G (catalog #A11001; 1:200, RRID: AB_2534069) were obtained from Life Technologies (Carlsbad, USA). 4′, 6-diamidino-2-phenylindole (DAPI; catalog #KGA215−10) was purchased from KeyGEN BioTECH (Nanjing, China). Alexa Fluor 488 conjugate dextran (catalog #D22910) was bought from Thermo Fisher Scientific (Waltham, USA). Protein A Agarose Beads (catalog #9863), Anti-rabbit IgG *H* + *L* DyLightTM 800 4X PEG (catalog #5470; 1:15, 000) and anti-mouse IgG *H* + *L* DyLightTM 680 (catalog #5151; 1:30, 000) were obtained from Cell Signaling Technology (Boston, USA).

2.2. Animals and animal experiments

Ethics: Animal experiments were approved by the Experimental Animal Center of Xuzhou Medical University (201802W007) and performed according to National Institutes of Health (NIH) Guide for the Care and Use of Laboratory Animals.

Rats: A total of 200 Sprague-Dawley adult male rats (8−10 weeks of age, 250±10 g, RRID: MGI: 5651135) were obtained from the Experimental Animal Center of Xuzhou Medical University. Rats were housed in a controlled environment (humidity, 50−60%), which maintained a 12-hour light/dark cycle. All animal procedures conform to National Institutes of Health (NIH) Guide for the Care and Use of Laboratory Animals, 8th edition [25]. The animal care and experimental protocols were approved by the Xuzhou Medical University Committee on Animal Care.

Treatment: All experiments conformed to the international guidelines on the ethical use of animals.

A closed-chest rat model of MI/R that supports direct intramyocardial gene delivery was performed as previously described [26]. Briefly, SD rats were anaesthetized with sodium pentobarbital (60 mg/kg) intraperitoneally and maintained under anesthesia using isoflurane (1.5−2.0%) mixed with air. After adequate anesthesia, the

animals were intubated with a 14-gage polyethylene catheter and ventilated with room air using a small animal ventilator (Model683: Harvard Apparatus, Boston, MA, USA). Following thoracotomy, a 6−0 prolene monofilament polypropylene sutures (Ethicon, Somerville, NJ) was passed from below to loop the LAD. The 2 ends of the prolene suture were fixed to PE-10 tubes. Next, another 6−0 prolene suture was knotted along the loop. Then, a PE-10 tube was fixed to its end. LR-AAV or LR-siRNA-AAV (2×10^{12} TU) prepared in 20μL Enhanced Infection Solution (ENIS, GeneChem, catalog #REVG0002) was delivered with a 20-μl syringe and 25-gage needle into the myocardium along the LAD. Then, the pleural cavity was closed under positive end-expiratory pressure following the evacuation of air inside the chest. After 3 weeks, the reserved line was tightened to establish the AMI model, and released the knot to achieve coronary recanalization. The AMI or AMI/R models were successfully established by ECG results. Sham-operated animals underwent an identical surgical procedure without artery ligation. All surgical procedures were performed under aseptic conditions.

Rats were euthanized by an intraperitoneal injection of sodium pentobarbital (a dosage of 150 mg/kg) in combinations with CNS depressants (phenytoin). And all animal euthanasia procedures conform to American Veterinary Medical Association (AVMA) Guidelines for the Euthanasia of Animals: 2020 Edition.

2.3. Preparation of adeno-associated viruses (AAV) and plasmids

AAVs were generated by the AAV Vector Unit at ICGEB Trieste (http://www.icgeb.org/avu-core-facility.html) following a protocol as previously described [27]. LR over-expression plasmids and the short interference RNA (siRNA) against LR, TIMAP and PP1cβ were successfully constructed by 293T cells, respectively. Human VE-cadherin (hVE-cad) CRISPR/Cas9 sgRNA, the wild-type (WT) hVE-cadherin, hVE-cad^{S665D} (phosphomimic), hVE-cad^{S665V} (phosphonull), LR CRISPR/Cas9 sgRNA, the wild-type (WT) LR, LR^{S43D}, LR^{Y47D}, LR$^{S75-78-79D}$, LR^{T125D} (phosphomimic) and LR^{S43A}, LR^{Y47A}, LR$^{S75-78-79A}$, LR^{T125A} (phosphonull) mutants were generated from Genechem (Shanghai, China). Plasmid carrying pCMV6-XL5-RPSA (LR) human cDNA clone was purchased from OriGene (Maryland, USA). All the adeno-associated viral vectors were constructed and labeled with green fluorescent protein (GFP). The concentrated titer of virus suspension was 2×10^{12} TU/L.

2.4. Cell culture and cell lines

HCMECs (Human Cardiac Microvascular Endothelial Cells, RRID: CVCL_U985, ScienCell, USA) were used between the third and fifth generation cultured in endothelial cell medium (ECM, ScienCell) containing 5% fetal bovine serum (FBS, ScienCell), 1% endothelial cell growth supplement (ECGS, ScienCell) and 1% penicillin/ streptomycin solution (ScienCell, USA) at 37 °C in a humidified atmosphere of 5% CO_2 and 95% air (20% oxygen). To induce the oxygen glucose deprivation (OGD) model, the glucose-free and serum-free medium (Gibco) replaced ECM and cells were placed into a tri gas incubator (Heal Force Bio-meditech Holdings, Ltd., Shanghai, China) with 94% N_2, 5% CO_2, and 1% O_2 for 4 h. In order to construct a stable cell line, lentivirus hVE-cad CRISPR/Cas9 sgRNA (MOI=20) and LR CRISPR/Cas9 sgRNA (MOI=10) were infected following the manufacturer's protocol at the desired multiplicity of infection when the fusion density of cells reached approximately 30−40%, respectively. Then infection medium was replaced with fresh medium after 8 h. After an additional 64 h, GFP co-expression on the construct was used to determine efficiency of viral transduction.

2.5. Myocardial PET perfusion study

Myocardial PET perfusion imaging with ^{13}N-NH_3 was conducted as previously described [28]. On brief, PET was performed by MITRO Biotech Co., Ltd. (NanJing, China). Micro PET (Siemens) dynamic scan was performed after ^{13}N-NH_3 (300±150 μCi) injection respectively.

$$\text{SUV} = \frac{\text{uptake of radioactive substances in the region of interest } (\mu\text{Ci /g})}{\text{total injection dose } (\mu\text{Ci })/\text{weight (g)}}$$

The animal models were randomly divided into six groups as follows: i) Sham group, surgical procedure without artery ligation; ii) AMI group, arterial ligation for 4 h; iii) AMI/ Recanalization (AMI/R), arterial ligation for 4 h + releasing the ligation immediately before PET scan; iv) AMI/*R* + Vector, arterial ligation for 4 h + releasing the ligation immediately before PET scan + Vector injection; v) AMI/*R* + LR, arterial ligation for 4 h + releasing the ligation immediately before PET scan + LR injection.

2.6. Immunofluorescence

The myocardial tissue frozen sections of rats and cells were fixed for 15 min with 4% paraformaldehyde, permeabilized with Triton X-100 (0.1%), following blockage with solution containing 5% bovine serum. Samples were incubated with anti-VE-cadherin; anti-CD31; anti-TIMAP; anti-PP1cβ for 12 h in 4 °C. Then the sections were incubated with secondary antibodies at 37 °C for 1 hour, containing Alexa Fluor 594 donkey anti-rabbit immunoglobulin G and Alexa Fluor 488 goat anti-mouse immunoglobulin G. In addition to the above procedures, cells incubated with LR/Alexa Fluor 350 Conjugated antibody at 37 °C for 4 h to detect colocalization. Nuclei were stained with DAPI (KeyGEN BioTECH, China) in the end. After final washing, 50% glycerin was used to mount coverslips on slides. Finally, sections were observed under a fluorescence microscope (Olympus, Tokyo, Japan) or confocal laser scanning microscope (Olympus).

2.7. Dextran perfusion experiment

Rats were anesthetized with pentobarbital 90 mg•kg^{-1} and 0.2 ml heparin via intraperitoneal injection. And the absence of the pedal reflex was considered as an indication that a surgical plane of anesthesia has been maintained. Then the hearts were taken off quickly and placed in ice-cold modified Tyrode's solution (in mmol/L) including 93 NaCl, 20 $NaHCO_3$, 1 Na_2HPO_4, 1 $MgSO_4$, 5 KCl, 1.8 $CaCl_2$, 20 Na-acetate, 20-glucose. The hearts were mounted on a Langendorff system with the aorta onto a cannula. Then modified Tyrode's solution was retrogradely perfused at 9 ml/min, containing 20 mg/ml Alexa Fluor^{TM}488 conjugate dextran. In addition, the hearts were harvested immediately for making frozen sections. Finally, sections were observed under a fluorescence microscope (Olympus, Tokyo, Japan).

2.8. Identification of phosphorylation sites in LR by LC−MS/MS analysis

The solution containing LR purified protein was digested with TPCK Immobilized Magnetic Trypsin (Clontec, Saint-Germain-en-Laye, France) for 90 min. The digestions were stopped by removing the magnetic beads and addition of TFA to a final concentration of 0.5%. Phosphopeptide enrichment was carried out using TiO_2 and Ti-IMAC. The tryptic peptides were dissolved in solvent A (0.1% formic acid in 2% acetonitrile), directly loaded onto a homemade reversed-phase analytical column packed with Reprosil-Pur Basic C18, 1.9 μm. The gradient was comprised of an increase from 2% to 22% solvent B (0.1% formic acid in 98% acetonitrile) over 40 min, 22% to 35% in 12 min and climbing to 80% in 4 min then holding at 80% for the last 4 min, all at a constant flow rate of 350 nL/min on an EASY-nLC 1000 UPLC system. The peptides were subject to NSI source followed by tandem mass spectrometry (MS/MS) in Q ExactiveTM Plus (Thermo Fisher Scientific, Waltham, MA, USA) coupled online to the UPLC. The *m/z* scan range was 350−1800 for the full scan, and intact peptides were detected in the Orbitrap at a resolution of 70,000. Peptides were then selected for MS/MS using NCE setting as 28 and the

fragments were detected in the Orbitrap at a resolution of 17,500. A data-dependent procedure that alternated between one MS scan followed by 20 MS/MS scans with 15.0 s dynamic exclusion. The automatic gain control (AGC) was set at 5E4. The fixed first mass was set as 100 *m/z*.

The LC-MS/MS data was searched against the Homo sapiens Uniprot database (version 2018) using the PEAKS (Matrix Science, UK) database search engine. Trypsin/P was specified as cleavage enzyme allowing up to 3 missing cleavages, 4 modifications per peptide and 5 charges. Monoisotopic peptide tolerance was set to 20 ppm, and fragment mass tolerance was set to 0.02 Da. Carbamidomethylation on Cys-was specified as fixed modification and oxidation on Met, phosphorylation on Ser, Thr, Tyr-and acetylation on protein N-terminal were specified as variable modifications. False discovery rate (FDR) thresholds for protein, peptide and modification site were specified at 1%.

2.9. Real-time reverse transcription-qPCR (RT-qPCR)

Total RNA was extracted with TRIzol reagent (Invitrogen) from HCMECs according to the manufacturer's instructions. Then the RNA (1000 nmol) was subjected to reverse transcription by the Prime Script RT reagent Kit with gDNA Eraser (TaKaRa). The mixture containing primers (Sangon Biotech, Shanghai, China) and 20-ul reactions was detected by Light Cycler 480II (Roche, Basel, Switzerland) using SYBR Green PCR Master Mix. Relative quantitative analysis of the change in expression levels was obtained using the ΔΔCT method and normalized to GAPDH. The sequences of the primer are as follows: 5′-GAAAGCAGTCTTTGGAAACCAT-3′ (PP1cβ forward), 5′-GAAGCATCTTTGGAAACCAT-3′ (PP1cβ reverse); 5′-GATGAGATGCCAATAGACCTGT-3′ (TIMAP forward), 5′-GCTGTGACTTCATGATCACATC-3′ (TIMAP reverse); 5′-CGAGATCCCTCCAAAATCAA-3′ (GAPDH forward), 5′-TGTGGTCATGAGTCCTTCCA −3′ (GAPDH reverse).

2.10. Permeability measurement in vitro

Cell-culture Trans-well inserts (Trans-well [12 mm diameter, 0.4 mm pore size]; Corning, Cambrige, MA) were used to detect permeability of monolayer cardiac microvascular endothelial cells. Before experimentation, cells were maintained at confluence on porous polyester membrane inserts and ECM (150 and 500 ul) were added into the upper and lower compartments, respectively. Then, the FITC-dextran (10 μmol/l) was added into the upper chamber. After OGD 4 h, the florescence intensities (excitation at 530 nm and emission at 590 nm) of samples were measured by Synergy2 multifunction microplate reader (BioTek, Vermont, USA) via 96-well cluster plates (black with clear bottoms, polystyrene, Corning Costar, USA). The FITC-dextran that passed across the endothelial cell monolayer was normalized to the fluorescence reading from the upper chamber, and permeability was calculated as relative fluorescence units.

2.11. Protein extraction

Cells were lysed with Cell Total Protein Extraction Kit (Sangon Biotech, Shanghai, China) for whole cell lysate. And for nuclear and cytoplasmic lysates, cells were extracted via Nuclear and Cytoplasmic Protein Extraction Kit (KeyGEN BioTECH, Shanghai, China) according to the manufacturer's instructions. Protein concentrations were measured using a Bicinchoninic Acid Assay Kit (BCA, Thermo Fisher Scientific, Inc.).

2.12. Western blot and co-immunoprecipitation

For western blot analysis, a total of 50 ng protein per lane was prepared and separated by 8−12% sodium dodecyl sulfate-polyacrylamide gel (SDS-PAGE) and electro-transferred to nitrocellulose membranes (Millipore, Darmstadt, Germany). Following blocking with 5% skim milk for 3 h at room temperature, the membranes were incubated with primary antibodies of phospho-Ser665-VE-cad, pY47-LR, pT125-LR, LR, PP1cβ, TIMAP, CD31, β-actin, Lamin A/C at 4 °C overnight. Then the membranes were incubated with fluorescently labeled secondary antibodies including anti-mouse or anti-rabbit antibodies (Li-Cor Biosciences, Lincoln, USA) at 2 h at room temperature. Finally, signals were detected by Odyssey Infrared Imaging System (Li-Cor Biosciences, Lincoln, USA). Digitized images were analyzed using Image J (NIH, Bethesda, USA). For all western blot analyses, other than when specifically noted, protein levels were calculated from the ratio of corresponding protein/β-actin.

For co-immunoprecipitation, the whole proteins of HCMECs were extracted using the special lysis buffer for immunoprecipitation. Part of the supernatant was used as input control and the rest was immunoprecipitated by rocking with 5 μg of anti-LR antibody and 50 ul agarose A protein overnight at 4 °C. The beads were washed 3 times with lysis buffer and boiled in 30 μl SDS sample buffer (62.5 mM Tris−HCl, 10% glycerol, 2% (w/v) sodium dodecyl sulfate [SDS], 5% 2-mercaptoethanol, and 10 g/ml bromophenol blue, pH 6.8). Finally, the supernatants were resolved by western blot.

2.13. PP1c activity assay

PP1c activity was calculated spectrophotometrically using Cell PP1c Colorimetry KIT (GENMED Scientifics, catalog #GMS 50313.1, Shanghai, China) according to the manufacturer's instructions [29]. Briefly, a series of 20 μl standards, controls and samples was added into a 96-well plate (Corning, New York, USA) at a concentration of 1×10^4 cells/ml. 10-ul Reagent A lysate buffer and 20-ul Reagent C buffer conjugated with malachite green fluorescent dye were mixed for 10 min at 37 °C. Then the mixture was discarded, and the wells were washed 3 times with Reagent B Cleaning Buffer. Reagent D and Reagent E were dispensed into each well, incubating for 20 min at 37 °C. Finally, reactions were stopped with 20-ul Reagent F stop solution. The absorbance at 660 nm was measured with a microplate reader (BioTek Synergy 2, Vermont, USA). The PP1c activity of each sample was calculated based on the standard curve.

2.14. Statistical analysis

For all quantitative analyses, other than when specifically noted, data are expressed as means ± SEM and repeated at least three times independent biological samples. Statistical significance was analyzed using GraphPad Prism (GraphPad Software Inc., San Diego, USA). Two-tailed Student's t tests were performed for two experimental groups, and one-way ANOVA was performed for three or more experimental groups. $P<0.05$ was considered as significant difference.

2.15. Role of funding source

The study design was approved by the Funder. The funders played no role in data collection, analysis, or interpretation of the data, or drafting of the manuscript. The corresponding author had full access to all the data in the study and had final responsibility for the decision to submit for publication.

3. Results

3.1. LR is closely related to the occurrence and severity of no-reflow in rat AMI/R models

In order to determine the detailed role of LR in the occurrence of no-reflow, intramyocardial LR-AAV and LR-siRNA gene delivery were performed in rat hearts, and AMI/R models were subsequently

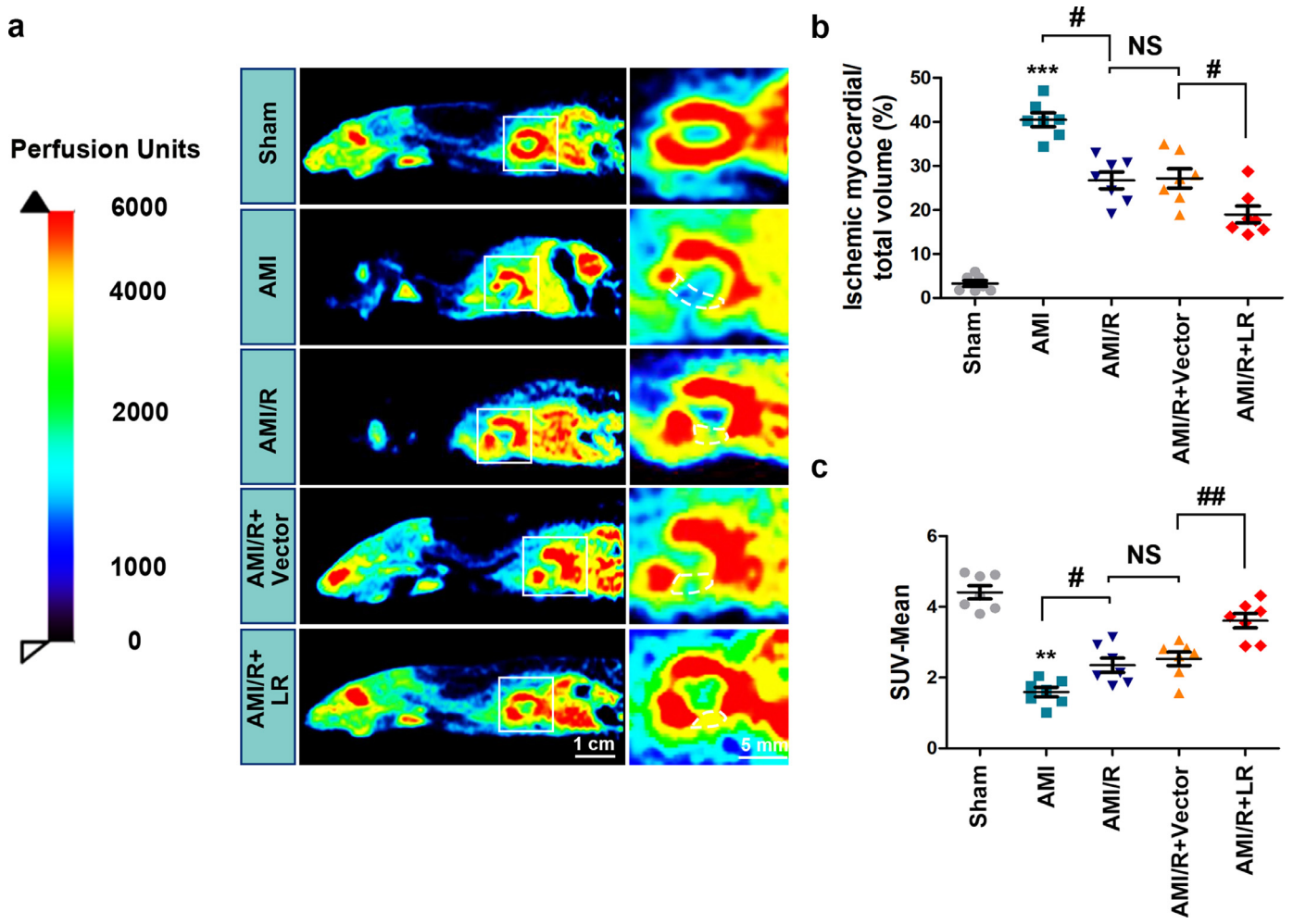

Fig. 1. LR is closely related to the occurrence and severity of no-reflow in rat AMI/R models. (a) Representative images of PET perfusion imaging with ^{13}N-NH$_3$. The ranges selected by the dashed indicate ischemic regions after AMI or ischemic/reperfusion regions after AMI/R, n = 7. (b) Quantification of ischemic myocardial total volume. (c) Quantification of mean-standard uptake value (SUV) of the hearts. $^{**}P<0.01$, $^{***}P< 0.001$ vs the sham group; $^{\#}P<0.05$, $^{\#\#}P<0.01$; NS, $P>0.05$ vs the indicated group. Data are presented as means ± SEM. Statistical analysis: One-way ANOVA with Tukey post-hoc (b, c). NS, no significant difference.

established (Fig. S1a and S1b). However, it was seen that siLR treatments usually caused serious arrhythmia at rest and sudden death during surgery (Supplementary Table). These results indicated that LR is an important regulator of the heart's internal environment and leads us to fail to demonstrate the effect of siLR treatment on AMI and no-reflow.

PET perfusion imaging with ^{13}N-NH$_3$ was performed after temporary coronary occlusion for 4 h (Fig. 1a). The results showed that blocking the LAD coronary artery caused serious myocardial hypoperfusion in AMI rats. After the ligation was lifted, significant no-reflow areas could be found in AMI/R rats in spite of epicardial coronary artery reperfusion. LR overexpression therapy was found to reduce the volume of ischemic myocardium (27.15 ± 2.17 [AMI/*R*+Vector group] versus 18.99 ± 1.90 [AMI/*R*+LR group], $P<0.05$, by Tukey's post hoc test) and increase the mean-SUV (2.51 ± 0.19 [AMI/*R*+Vector group] versus 3.30 ± 0.15 [AMI/*R*+LR group], $P<0.01$, by Tukey's post hoc test) (Fig. 1b and 1c). In other words, a high level of LR can effectively reduce the no-reflow area after coronary recanalization.

3.2. LR promotes the stability of AJs and endothelial barrier via down-regulating phospho-Ser665-VE-cadherin

The destructions of microvascular structure and function are the main pathogenesis of no-reflow. In vivo, dextran perfusion experiment was performed to determine the effects of ischemia and LR over-expression on vascular permeability. The results indicated that ischemia for 4 h caused serious dextran leakage, while LR over-expression treatment significantly improved this process ($P<0.05$, by Tukey's post hoc test) (Fig. S2a and S2c). Immunofluorescence analysis showed that VE-cadherin labeling created a linear signal in the sham group (the protein is uniformly distributed on the membrane), while loosely distributed in the AMI/R and AMI/*R*+Vector group (internalization of VE-cadherin induced by ischemia). However, the inorganized VE-cadherin was partly reversed after LR over-expression treatment (Fig. S2b).

Thereafter, focused analyses were performed on the endothelial adherens junctions and endothelial permeability by immunofluorescence and the trans-well system in HCMECs (Fig. 2a and 2b). Similarly, the data in vitro showed that LR over-expression could decrease the hypoxia-induced internalization of VE-cadherin and maintained the endothelial barrier. Consistent with previous reported, we also found that the hypoxia-induced internalization of VE-cadherin was mainly via increasing the phospho-Ser665-VE-cad (Fig. S3). Western blot analysis showed that LR overexpression significantly down-regulated the level of phospho-Ser665-VE-cad and internalized-VE-cadherin (Fig. 2c). Next, VE-cadherin mutants that mimicked the phosphorylated states (hVE-cad^{S665D}) were designed to analyze whether LR inhibits the endocytosis of VE-cadherin by reducing phospho-Ser665-VE-cad, and the results showed that the

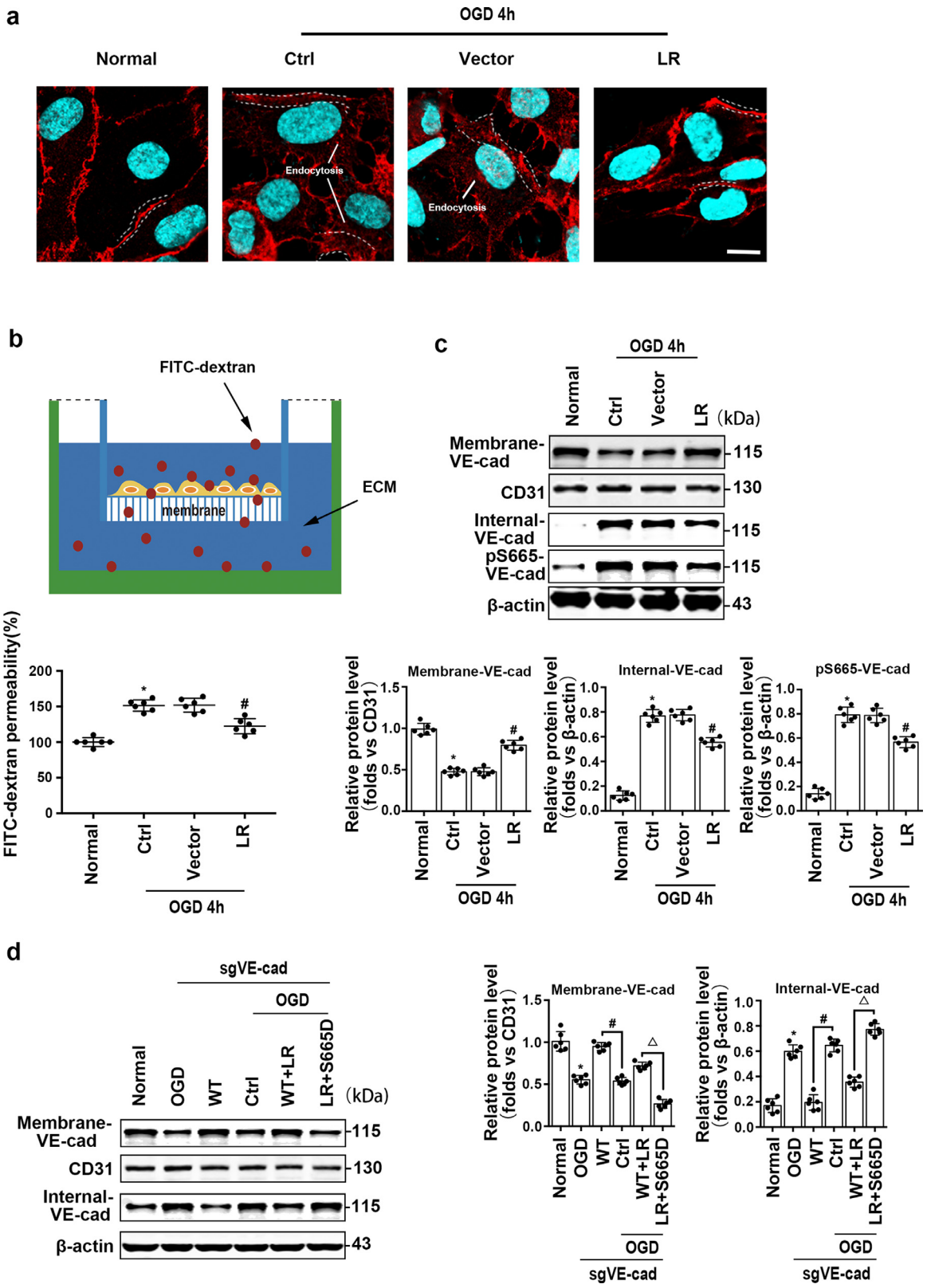

Fig. 2. LR promotes the stability of AJs and endothelial barrier via down-regulating phospho-Ser665-VE-cadherin. (a) Representative confocal immunofluorescence images of VE-cadherin in HCMECs with corresponding treatments, bar=5 μm. (b) Trans-well for permeability of the endothelial cell. $^{*}P<0.05$ vs the normal group; $^{\#}P<0.05$ vs the OGD control group, n = 6. (c) Western blot analysis for the expression of membrane-VE-cad, internal-VE-cad, pS665-VE-cad. $^{*}P<0.05$ vs the normal group; $^{\#}P<0.05$ vs the OGD control group, n = 6. (d) Western blot for membrane-VE-cad, internal-VE-cad with corresponding treatments. $^{*}P<0.05$ vs the normal group; $^{\#}P<0.05$, $^{\triangle}P<0.01$ vs the indicated group, n = 6. Data are presented as means ± SEM. Statistical analysis: One-way ANOVA with Tukey post-hoc (b-d). AJs, adherens junctions; NS, no significant difference.

activity of LR to inhibit the internalization of VE-cadherin was significantly blocked by hVE-cad^{S665D} (Fig. 2d). Such evidences prompted us to hypothesize that LR is involved in the transmission of this phosphorylation signal.

3.3. The phosphorylation of LR amino acid residues, TYR 47 and THhrh 125, contributes to phospho-Ser665-VE-cad

The above results indicate that LR plays an important role in maintaining the stability of vascular structure and function and reducing no-reflow. Western blot and PCR analysis indicated that OGD treatment had little effect on the expression level of LR in HCMECs (Fig. 3a and 3b). Results of LC-MS/MS analysis demonstrated that OGD 4 h induced phosphorylation of LR at residues Ser43 (Ser43-LR), Tyr47 (Y47-LR), Ser75-78-79 (S75-78-79-LR), and Thr125 (T125-LR) (Fig. 3c). Western blot analysis was performed to further proved the level of phospho-Ser43-LR (pS43-LR), phospho-Tyr47-LR (pY47-LR), phospho-Ser75-78-79-LR (pS75-78-79-LR) and phospho-Thr125-LR (pT125-LR) were significantly increased in OGD 4 h group (Fig. 3d).

3.4. Y47-LR is the upstream target site for T125-LR in the regulation of the phospho-Ser665-VE-cad-related signaling pathway

Next, LR mutants containing LR^{S43D} (phosphomimic), LR^{Y47D} (phosphomimic), LR$^{S75-78-79D}$ (phosphomimic), and LR^{T125D} (phosphomimic) and LR^{S43A} (phosphonull), LR^{Y47A} (phosphonull), LR$^{S75-78-79A}$ (phosphonull), and LR^{T125A} (phosphonull) were engineered to

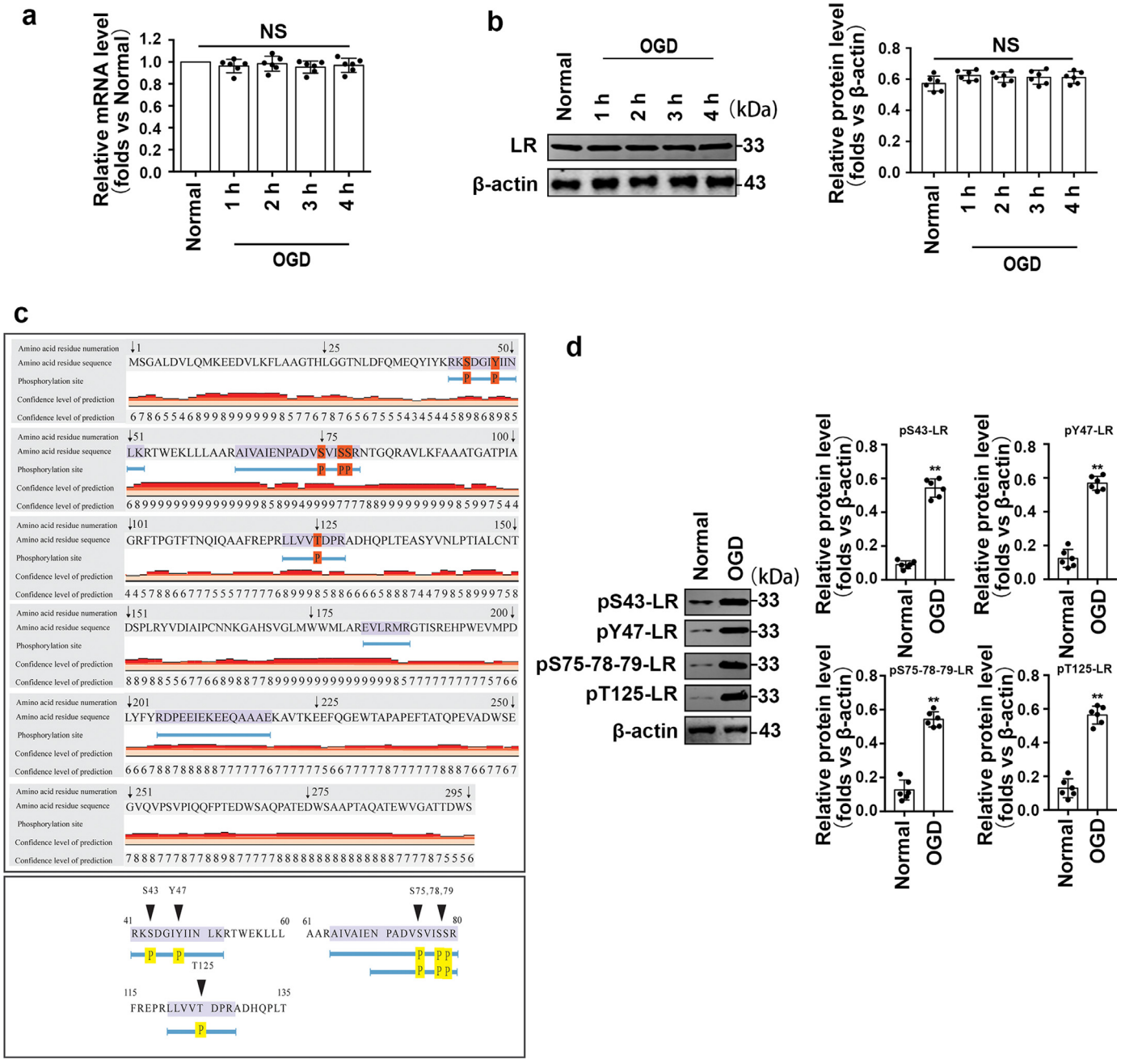

Fig. 3. The phosphorylation of LR amino acid residues, Tyr 47 and Thr 125, contributes to phospho-Ser665-VE-cadherin. (a) RT-qPCR analysis for LR mRNA expression in HCMECs. (b) Verification of LR expression, NS, $P>0.05$ vs the indicated group, $n = 6$. (c) LC−MS/MS analysis for the phosphorylation residues of LR in endothelial cells. (d) Western blot analysis for the expression of pS43-LR, pY47-LR, pS75−78−79-LR and pT125-LR, $^{**}P<0.01$ vs the respective normal group, $n = 6$. Statistical analysis: One-way ANOVA with Tukey post-hoc (a, b); Student's T-test (d). NS, no significant difference; pS665-VE-cad, phospho-Ser665-VE-cad.

demonstrate the core role of LR in regulating phospho-Ser665-VE-cad. Under OGD, LR^{Y47A} and LR^{T125A} treatment rather than LR^{S43A} treatment and $LR^{S75\text{-}78\text{-}79A}$ treatment effectively inhibited the level of phospho-Ser665-VE-cad in HCMECs (Fig. 4a and 4b). To more clearly understand the relationship between pY47-LR and pT125-LR in this complex phosphorylation signal, the expression of pY47-LR and pT125-LR under several conditions were further detected. Specifically, LR^{T125D} treatment could lead to a significant increase in the expression of phospho-Ser665-VE-cad under normoxic condition (0.91 ± 0.07 [LR^{T125D} group] versus 0.11 ± 0.02 [WT group], $P<0.05$, by Tukey's post hoc test), while LR^{Y47D} treatment could not [0.13 ± 0.02 [LR^{Y47D} group] versus 0.11 ± 0.02 [WT group], $P>0.05$, by Tukey's post hoc test) (Fig. 4c). These data indicated that pT125-LR, rather than pY47-LR can directly cause phospho-Ser665-VE-cad independent of hypoxia environment. Under 4 h of OGD treatment, the level of phospho-Ser665-VE-cad in LR^{Y47D} and LR^{T125D} groups were significantly increases compared with the WT group ($P<0.05$, by Tukey's post hoc test). However, LR^{Y47D} combined with LR^{T125A} treatment significantly decreased the level of phospho-Ser665-VE-cad, while LR^{Y47A} combined with LR^{T125D} has no effect on the level of phospho-Ser665-VE-cad (Fig. 4d). These results revealed that the regulation of pY47-LR on the level of phospho-Ser665-VE-cad is dependent on anoxic environment or pT125-LR. Hence, Y47-LR may be the upstream target site for T125-LR in this series of complex phosphorylation cascades signals.

3.5. The role of PP1c in the regulation pT125-LR

The dynamic balance between activities of protein kinases and phosphatases is the most common mechanism for signal transduction. PP1 is highly expressed in endothelial cells and may participate in regulation of the phospho-LR-related signaling pathway [19,30]. It was found that LR over-expression and siLR treatment had little effect on the expression of PP1c at both protein and RNA level in HCMECs. Further analysis showed that OGD 4 h treatment induced PP1c transfer from cell membrane to cytoplasm and nucleus, and LR over-expression could reversed this process (Fig. S4a and S4b). Moreover, our data also indicated that there was a positive correlation between the activity of PP1c and the expression level of PP1c on cell membrane (Fig. S4c). Western blot and immunofluorescence analysis showed that LR^{Y47A} treatment could increase the expression of PP1c in the plasma membrane compared with the control and OGD 4h-treated WT groups. In contrast, LR^{Y47D}, LR^{T125A} and LR^{T125A} treatments had no effects on the expression level of PP1c in the plasma membrane (Fig. 5a and 5b). In addition, LR^{Y47A} treatment significantly reduced the level of pT125-LR, which further proved that Y47-LR is the upstream node of T125-LR. The application of PP1c inhibitor Microcystin-LR (Mic-LR) [31] or siPP1c treatment could significantly block the down-regulation of pT125-LR after LR^{Y47A} treatment (Fig. S4d and S4e).

In brief, the pY47-LR determines the recruitment of PP1c on the membrane. PP1c in the plasma membrane is involved in the regulation of the phosphorylation or dephosphorylation of T125-LR.

3.6. The role of TIMAP in the regulation pT125-LR

TIMAP, a specific targeting subunit of PP1c, not only determines the subcellular location and substrates of PP1c, but also regulates the catalytic activity of PP1c [32]. Therefore, focused studies were conducted on TIMAP. The results of PCR and western blotting showed that OGD 4 h, LR over-expression and siLR treatment had little effect on the level of TIMAP in HCMECs (Fig. S5a and S5b). Furthermore, western blot and immunofluorescence analysis showed that OGD 4 h treatment induced TIMAP transfer from cell membrane to cytoplasm, and LR^{Y47A} treatment could reversed this process (Fig. 5c and 5d). Notably, siTIMAP treatment significantly blocked the down-regulation of pT125-LR after LR^{Y47A} treatment, which may be achieved by reducing PP1c recruitment in the plasma membrane rather than reducing PP1c expression in HCMECs (Fig. S5c-S5e). Therefore, we believe that it is TIMAP and PP1c which jointly mediate the regulation of pY47-LR on the level of pT125-LR.

3.7. A novel LR-TIMAP/PP1c complex is responsible for the regulation of hypoxia-induced pT125-LR

Next, the close cross-linking and interaction between TIMAP/PP1c and LR promoted us to make a reasonable assumption that TIMAP/PP1c inhibits the level of pT125-LR by binding to LR. To identify the relationship between LR, TIMAP and PP1c, immunoprecipitation was performed to pull down TIMAP and PP1c from endothelial cell lysates with the specific LR antibody. The combination of LR, TIMAP and PP1c was detected in normal HCMECs, and OGD 4 h treatment caused a significant decrease in the levels of PP1c and TIMAP bound to LR (Fig. 6a, Fig. S6a and S6b). In addition, it was also found that LR^{Y47A} delivery could reverse the decline of TIMAP and PP1c binding on LR induced by OGD 4 h treatment (Fig. 6b). Confocal laser scanning microscope and co-immunoprecipitation were performed to further determine the effect of pY47-LR on the level of LR-TIMAP/PP1c complex. The results showed that high level of pY47-LR (induced by OGD or LR^{Y47D} treatment) inhibited the binding of LR, TIMAP and PP1c, while low level of pY47-LR (induced by LR^{Y47A}) significantly increase their binding (Fig. 6c). As shown in Fig. 6d, we provided an illustration to better understand the related molecular mechanism.

3.8. Low levels of pY47-LR and pT125-LR reduce no-reflow area in vivo

To evaluate the roles for the phosphorylation of LR in the occurrence and severity of no-reflow in vivo, we employed AMI/R models with intramyocardial gene delivery. As shown in Fig. 7a-7c, LR^{Y47A} and LR^{T125A} treatments equally reduce the volume of ischemic myocardium and increase myocardial perfusion level. These findings provided compelling evidence for low levels of pY47-LR and pT125-LR inhibit no-reflow phenomenon in vivo.

4. Discussion

At present, how to better prevent, manage and deal with no-reflow phenomenon after percutaneous coronary intervention (PCI) is the common focus of cardiovascular doctors and researchers all around the world. Here, we introduced the role of LR and the specific phosphorylation signaling process involved in LR in the development of the occurrence and development of no-reflow, and demonstrated an unknown LR-TIMAP/PP1c complex, whose stability can inhibit hypoxia-induced phosphorylation of VE-cadherin, thereby protecting the structure and function of microvessels.

The pathogenetic components of no-reflow are very complicated. Experimental studies have shown that there is clear evidence of microvascular injury, such as local swelling of endothelium and cardiomyocytes, breaks in the endothelial continuum, microvascular hemorrhage, thrombosis, interstitial edema, and inflammation in no-reflow zones. Clearly, these pathological changes are closely related to hypoxia-induced microvascular damage and together lead to no-reflow. The stability of endothelial AJs is critical to the maintenance of the vascular homeostasis and vascular function. Julie Gavard et al. and our previous study indicated that the phospho-Ser665-VE-cad greatly contribute to the internalization of VE-cadherin and the collapse of AJs [33]. The level of phospho-Ser665-VE-cad can be used as a marker for assessing microvascular structure and function in AMI. In this study, we further confirmed that the phosphorylation of VE-cadherin is closely related to microvascular dysfunction and no-reflow, and found that LR is a crucial regulator and participator in this process.

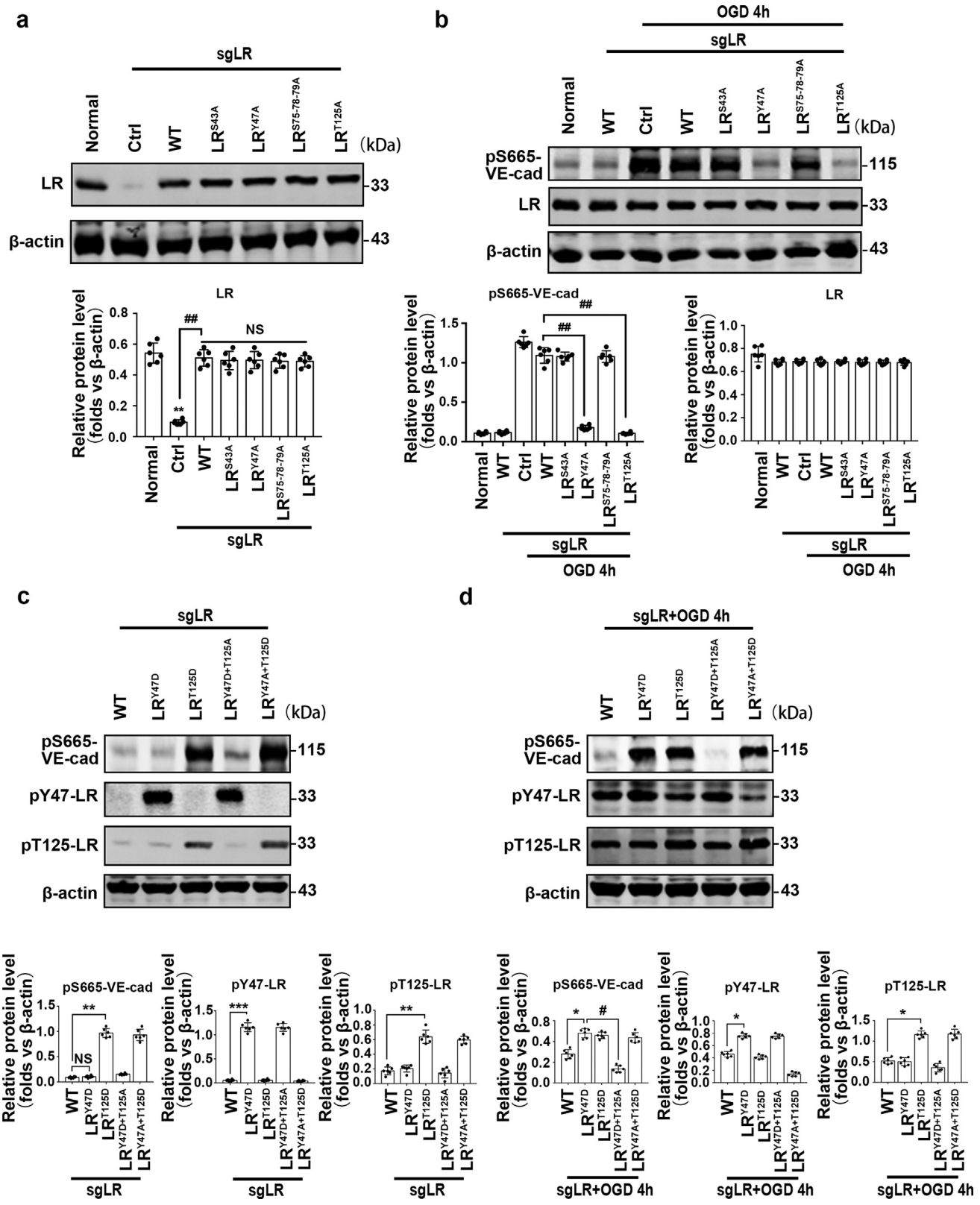

Fig. 4. Y47-LR is the upstream target site for T125-LR in the regulation of the phospho-Ser665-VE-cad-related signaling pathway. (a) Western blot analysis for the expression of LR in HCMECs with corresponding treatments. $^{**}P<0.01$ vs the normal group; $^{\#}P<0.05$, NS, $P>0.05$ vs the indicated groups, $n = 6$. (b) Western blot analysis for the expressions of pS665-VE-cad and LR in OGD 4h-treated HCMECs. $^{\#\#}P<0.01$ vs the indicated group, $n = 6$. (c, d) Western blot analysis for the expressions of pS665-VE-cad, pY47-LR and pT125-LR in HCMECs with corresponding treatments. $^{*}P<0.05$, $^{**}P<0.01$, $^{***}P<0.001$, $^{\#}P<0.05$, NS, $P>0.05$ vs the indicated group, $n = 6$. Statistical analysis: Data are presented as means ± SEM, one-way ANOVA with Tukey post-hoc (a-d). pS665-VE-cad, phospho-Ser665-VE-cad; pY47-LR, phospho-LR-Tyr47; pT125-LR, phospho-LR-Thr125; NS, no significant difference.

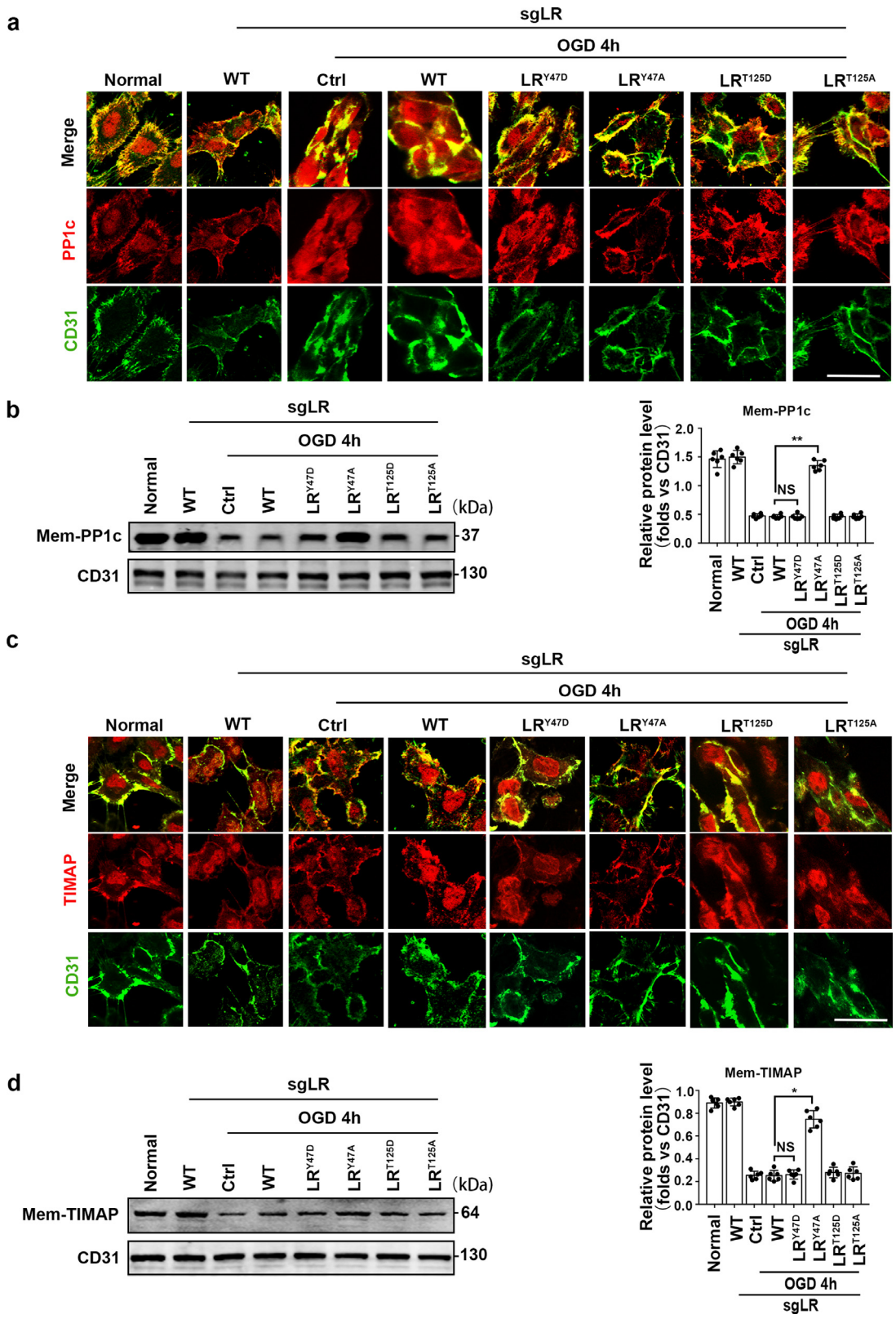

Fig. 5. The role of PP1c and TIMAP in the regulation pT125-LR by pY47-LR. (a) Immunofluorescence for PP1c (Red) and CD31 (Green) in HCMECs. bar=10 μm. (b) Western blot analysis for the expression level of PP1c in the plasma membrane. $^{**}P<0.01$, NS, $P>0.05$ vs the indicated group, $n = 6$. (c) Immunofluorescence staining was used to assess the localization of TIMAP (Red), bar=10 μm. (d) Western blot analysis for the expression level of TIMAP in the plasma membrane. $^{*}P<0.05$, NS, $P > 0.05$ vs the indicated group, $n = 6$. Statistical analysis: Data are presented as means ± SEM, one-way ANOVA with Tukey post-hoc (b, d). NS, no significant difference.

LR is closely involved in the development of early embryonic heart [34]. Here, our data indicated that LR is related to the occurrence and severity of no-reflow. In vivo, LR over-expression treatments could effectively protect the integrity of the endothelial barrier under ischemic injury, and relieve the reduction of tissue perfusion and the no-reflow area. In vitro, LR over-expression partly

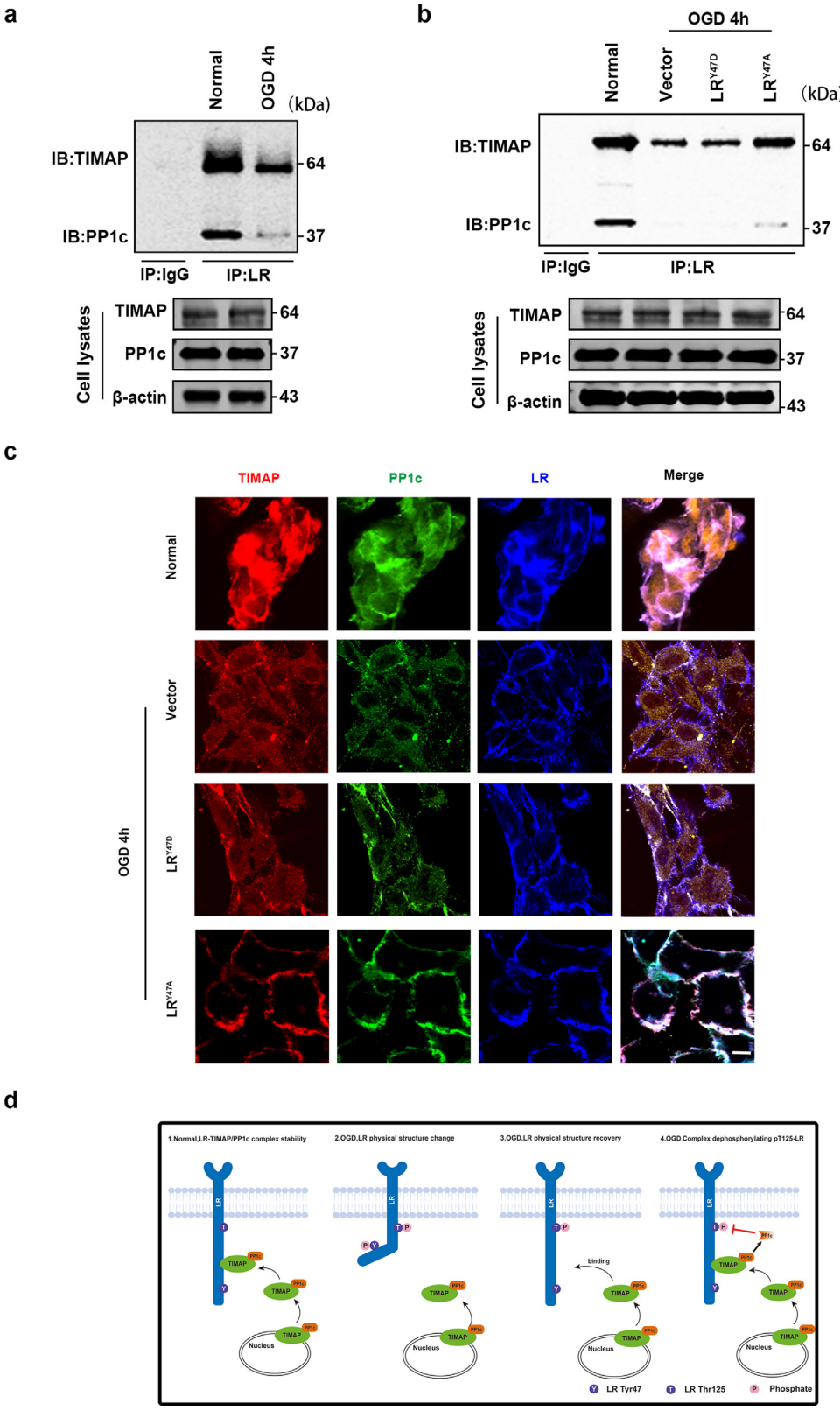

Fig.. 6. A novel LR-TIMAP/PP1c complex is responsible for the regulation of hypoxia-induced pT125-LR. (a) Immunoprecipitated analysis for the interactions between LR and TIMAP/PP1c respectively from HCMECSs lysates. Blots were probed for TIMAP and PP1c, $n = 4$. (b) HCMECSs were treated with LR^{Y47D} or LR^{Y47A}, then immunoprecipitated with LR antibody, $n = 4$. (c) Confocal immunofluorescence analysis of LR (Blue) interaction with TIMAP (Red) / PP1c (Green), Scale bar=5 μm. (d) Schematic representations in the setting of normoxia and OGD that phosphorylation or dephosphorylation of Y47-LR affects the stability of LR-TIMAP/PP1c to dephosphorylate pT125-LR. pT125-LR, phospho-LR-Thr125.

reverse the increase of level of phospho-Ser665-VE-cad and endothelial cell permeability. However, we noticed that hypoxia had little effect on the expression of LR in both protein and RNA level. Hence, the hypoxia-induced phosphorylation of VE-cadherin may be due to the histone modification rather than the decrease of LR expression.

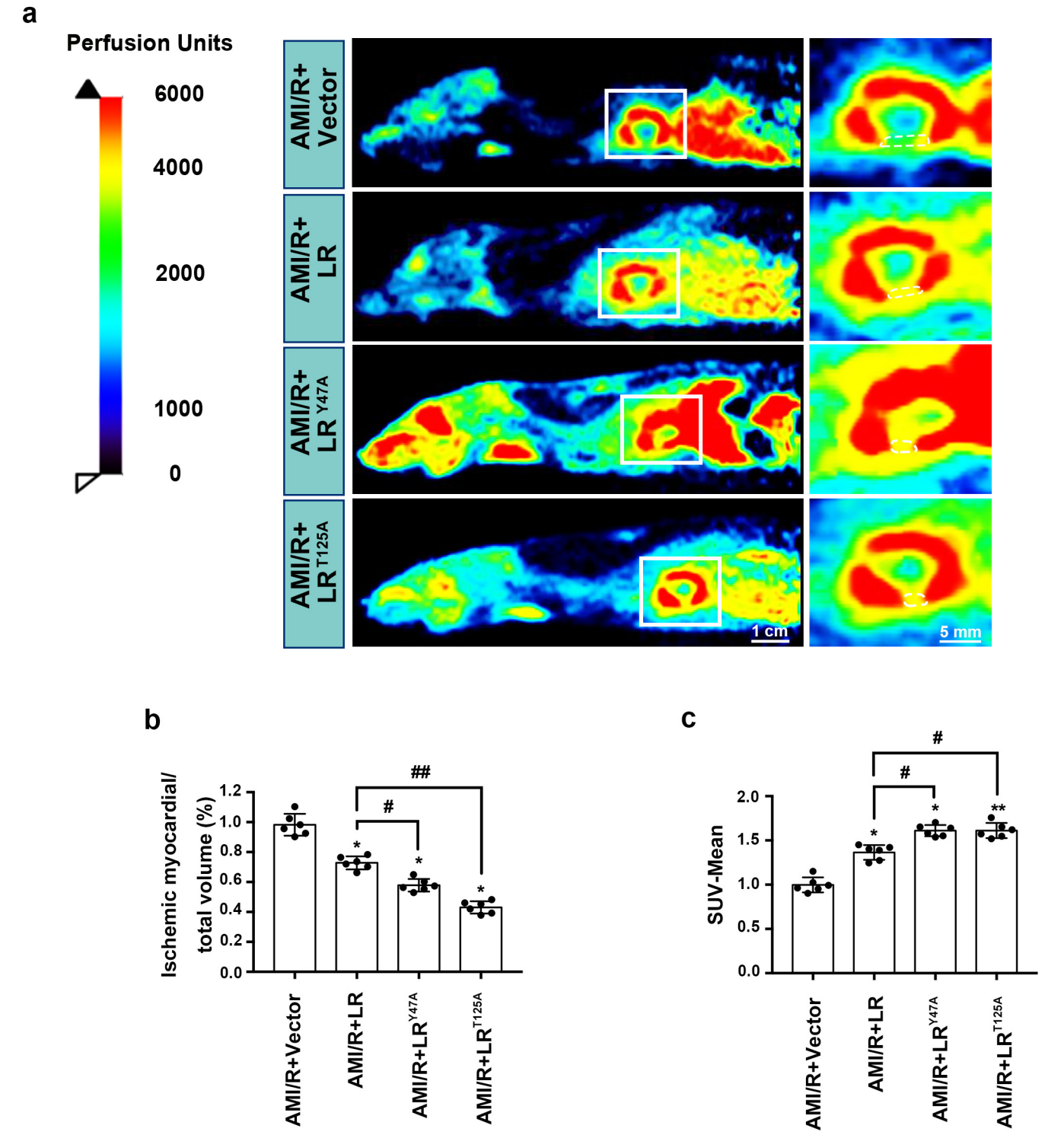

Fig. 7. Low levels of pY47-LR and pT125-LR Reduce no-reflow area in vivo. (a) Representative images of PET perfusion imaging with ^{13}N-NH_3. The ranges selected by the dashed indicate ischemic regions after AMI or ischemic/reperfusion regions after AMI/R, $n = 6$. (b) Quantification of ischemic myocardial total volume. (c) Quantification of main Standard uptake value (SUV) mean of the hearts. $^{*}P<0.05$, $^{**}P< 0.01$ vs the AMI/R+Vector group; $^{\#}P<0.05$, $^{\#\#}P<0.01$ vs the indicated group. Statistical analysis: Data are presented as means ± SEM, one-way ANOVA with Tukey post-hoc (b, c). NS, no significant difference.

The reversible phosphorylation of proteins is important in intercellular-communication [35]. LR, as a multifunctional protein in eukaryotes, can carry out some functions by phosphorylation. In fact, OGD 4 h treatment has caused significant increases in the level of pY47-LR and pT125-LR, which were subsequently proved to be important procedures for hypoxia-induced phospho-Ser665-VE-cad. Notably, we also found that pT125-LR and pY47-LR are not parallel in relationship in this signaling pathway. Specifically, p125T-LR seems to be a direct effector for phospho-Ser665-VE-cad. LR^{T125D} rather than LR^{Y47D} treatment spontaneously trigger phospho-Ser665-VE-cad in the absence of the OGD environment. In other words, pT125-LR can directly lead to phospho-Ser665-VE-cad independently of hypoxic environment. In addition, the increase of phospho-Ser665-VE-cad caused by OGD depends on pT125-LR and pY47-LR. LR^{T125D}

and LR^{Y47D} treatments could aggravate the phospho-Ser665-VE-cad caused by OGD 4 h treatment. Moreover, LR^{T125A} treatment almost completely reversed the synergistic effect of OGD and LR^{Y47D} at the level of phospho-Ser665-VE-cad. These results together support the argument that Y47-LR may be the upstream target site for T125-LR in the regulation of this phosphorylation cascade signaling pathway.

Mechanistically, we found that pY47-LR can reduce the recruitment of PP1c in the plasma membrane, which was responsible for the regulation of pT125-LR. As we know, reversible protein phosphorylation, regulated by the dynamic balance between the activities of protein kinases and phosphatases, is the most common mechanism for signal transduction [36,37]. One particularly promising candidate protein in this regard is TIMAP/PP1c, a functional complex. Cohen Pt et al. proposed that TIMAP mediates the subcellular localization and substrate of PP1c, and is involved in regulating its catalytic activity [32]. Little is known about the potential protein binding with TIMAP, but LR is one of its potential substrates [34,38,39]. Previous studies demonstrated that TIMAP containing the fourth ankyrin repeat (ANK 4) could be pulled down by LR, enabling PP1c to regulate LR phosphorylation [24]. Here, we first showed that TIMAP/PP1c can combine with LR on the cell membrane to form a novel LR-TIMAP/PP1c complex. This mode allows PP1c to effectively bind and modify its substrate LR. In other words, the formation of this complex activated the protein phosphatase activity of PP1c and regulated pT125-LR. Unsurprisingly, pY47-LR activates pT125-LR actually by inhibiting the formation of the LR-TIMAP/PP1c complex. Relevant data suggests that the phosphorylated modification states of Y47-LR determined the stabilities of LR-TIMAP/PP1c complex, indicating a causal link between pY47-LR and the complex. Based on this data, we made a reasonable hypothesis: Hypoxia-induced pY47-LR causes a change in the spatial conformation of LR, leading to the concealment or destruction of TIMAP binding region on LR. Certainly, more evidence and research is needed to support this conjecture.

Notably, the results of PET indicated that LR^{T125A} and LR^{Y47A} treatments showed better potency in reducing no-reflow compared with LR over-expression treatment. It emphasizes that maintaining the stability of the LR-TIMAP/PP1c complex is a priority over increasing the formation of this complex when dealing with no-reflow. Many evidences from in vitro experiments also support this argument.

Non-phosphorylated TIMAP exists in the nucleus and cytoplasm, while prenylated and phosphorylated forms of TIMAP are located predominantly on the membrane [21,40]. Indeed, we merely focus our attention on the distribution and interactions of TIMAP/PP1c under respective conditions, and the precise molecular mechanism on regulating the phosphorylation or prenylation of TIMAP, has not been illuminated, which is worthy of further investigation.

Generally, our findings demonstrate that low level of phospho-LR reduces no-reflow area through stabilizing the LR-TIMAP/PP1c complex and promoting the stability of AJs and endothelial barrier. The LR-dependent molecular mechanism has significant potential to open up new therapeutic avenues that target stabilizing endothelial barrier integrity to curb acute myocardial infarction and no-reflow.

Contributors

XYQ, HZ, and XCL conceived the project. XYQ, XCL, XCQ, YZW, TS, ZML, LDZ, JLC, YQZ, and SS performed the experiments. All authors contributed to experimental design and data analysis. XYQ, and XCL composed the manuscript. HZ and ZMZ verified the underlying data. All authors contributed to the writing and approved the final version of this manuscript.

Data sharing statement

All relevant data have been presented in the manuscript. All requests for or questions about the data can be initiated by contacting zhanghao@xzhmu.edu.cn.

Funding

This study was supported by funds from the National Natural Science Foundation of China (81870235 and 81400227), the Social Development Projects of Key R&D Programs in Jiangsu Province (BE2019643), the National Natural Science Foundation of Jiangsu Province (BK20171178), General Program of Jiangsu Commission of Health (H2017083), and the Project of Jiangsu Provincial Medical Youth Talent (QNRC2016778)

Declaration of Competing Interest

The authors declare that they have no competing interests.

Acknowledgments

We thank the National Natural Science Foundation of China, Natural Science Foundation of Jiangsu Province, and Xuzhou Municipal Science and Technology Bureau for their financial support. We thank all members of Thoracic Surgery Laboratory of Xuzhou Medical University for useful discussions.

Supplementary materials

Supplementary material associated with this article can be found in the online version at doi:10.1016/j.ebiom.2021.103251.

References

[1] Bordy R, Totoson P, Prati C, Marie C, Wendling D, Demougeot C. Microvascular endothelial dysfunction in rheumatoid arthritis. Nat Rev Rheumatol 2018;14(7):404–20.
[2] Galley HF, Webster NR. Physiology of the endothelium. Br J Anaesth 2004;93(1):105–13.
[3] Huveneers S, Daemen MJ, Hordijk PL. Between Rho(k) and a hard place: the relation between vessel wall stiffness, endothelial contractility, and cardiovascular disease. Circ Res 2015;116(5):895–908.
[4] Jr. Kushner FG, Hand M, Smith SC, King SB, 3rd Anderson JL, Antman EM, et al. 2009 focused updates: ACC/AHA guidelines for the management of patients with ST-elevation myocardial infarction (updating the 2004 guideline and 2007 focused update) and ACC/AHA/SCAI guidelines on percutaneous coronary intervention (updating the 2005 guideline and 2007 focused update) a report of the American College of Cardiology Foundation/American Heart Association Task Force on practice guidelines. J Am Coll Cardiol 2009;54(23):2205–41.
[5] Levine GN, Bates ER, Blankenship JC, Bailey SR, Bittl JA, Cercek B, et al. 2015 ACC/AHA/SCAI focused update on primary percutaneous coronary intervention for patients with ST-elevation myocardial infarction: an update of the 2011 ACCF/AHA/SCAI guideline for percutaneous coronary intervention and the 2013 ACCF/AHA guideline for the management of ST-elevation myocardial infarction: a report of the American College of Cardiology/American Heart Association Task Force on clinical practice guidelines and the society for cardiovascular angiography and interventions. Circulation 2016;133(11):1135–47.
[6] Fernandez-Martin L, Marcos-Ramiro B, Bigarella CL, Graupera M, Cain RJ, Reglero-Real N, et al. Crosstalk between reticular adherens junctions and platelet endothelial cell adhesion molecule-1 regulates endothelial barrier function. Arterioscler Thromb Vasc Biol 2012;32(8):e90–102.
[7] Komarova YA, Kruse K, Mehta D, Malik AB. Protein interactions at endothelial junctions and signaling mechanisms regulating endothelial permeability. Circ Res 2017;120(1):179–206.
[8] Kruse K, Lee QS, Sun Y, Klomp J, Yang X, Huang F, et al. N-cadherin signaling via Trio assembles adherens junctions to restrict endothelial permeability. J Cell Biol 2019;218(1):299–316.
[9] Kugelmann D, Rotkopf LT, Radeva MY, Garcia-Ponce A, Walter E, Waschke J. Histamine causes endothelial barrier disruption via Ca(2+)-mediated RhoA activation and tension at adherens junctions. Sci Rep 2018;8(1):13229.
[10] Colas-Algora N, Garcia-Weber D, Cacho-Navas C, Barroso S, Caballero A, Ribas C, et al. Compensatory increase of VE-cadherin expression through ETS1 regulates endothelial barrier function in response to TNFalpha. Cell Mol Life Sci 2020;77(11):2125–40.
[11] Vestweber D, Winderlich M, Cagna G, Nottebaum AF. Cell adhesion dynamics at endothelial junctions: VE-cadherin as a major player. Trends Cell Biol 2009;19(1):8–15.
[12] Dejana E, Vestweber D. The role of VE-cadherin in vascular morphogenesis and permeability control. Prog Mol Biol Transl Sci 2013;116:119–44.
[13] DiGiacomo V, Meruelo D. Looking into laminin receptor: critical discussion regarding the non-integrin 37/67-kDa laminin receptor/RPSA protein. Biol Rev Camb Philos Soc 2016;91(2):288–310.

[14] Yurchenco PD. Basement membranes: cell scaffoldings and signaling platforms. Cold Spring Harb Perspect Biol 2011;3(2).
[15] Bernard A, Gao-Li J, Franco CA, Bouceba T, Huet A, Li Z. Laminin receptor involvement in the anti-angiogenic activity of pigment epithelium-derived factor. J Biol Chem 2009;284(16):10480–90.
[16] Donaldson EA, McKenna DJ, McMullen CB, Scott WN, Stitt AW, Nelson J. The expression of membrane-associated 67-kDa laminin receptor (67LR) is modulated in vitro by cell-contact inhibition. Mol Cell Biol Res Commun 2000;3(1):53–9.
[17] Khusal R, Da Costa Dias B, Moodley K, Penny C, Reusch U, Knackmuss S, et al. In vitro inhibition of angiogenesis by antibodies directed against the 37kDa/67kDa laminin receptor. PLoS ONE 2013;8(3):e58888.
[18] Brautigan DL. Protein Ser/Thr phosphatases–the ugly ducklings of cell signalling. FEBS J 2013;280(2):324–45.
[19] Cao W, Mattagajasingh SN, Xu H, Kim K, Fierlbeck W, Deng J, et al. TIMAP, a novel CAAX box protein regulated by TGF-beta1 and expressed in endothelial cells. Am J Physiol Cell Physiol 2002;283(1):C327–37.
[20] Peti W, Nairn AC, Page R. Folding of intrinsically disordered protein phosphatase 1 regulatory proteins. Curr Phys Chem 2012;2(1):107–14.
[21] Boratko A, Gergely P, Csortos C. RACK1 is involved in endothelial barrier regulation via its two novel interacting partners. Cell Commun Signal 2013;11(1):2.
[22] Parmryd I, Andersson B, Dallner G. Protein prenylation in spinach chloroplasts. Proc Natl Acad Sci U S A 1999;96(18):10074–9.
[23] Wang M, Casey PJ. Protein prenylation: unique fats make their mark on biology. Nat Rev Mol Cell Biol 2016;17(2):110–22.
[24] Kim K, Li L, Kozlowski K, Suh HS, Cao W, Ballermann BJ. The protein phosphatase-1 targeting subunit TIMAP regulates LAMR1 phosphorylation. Biochem Biophys Res Commun 2005;338(3):1327–34.
[25] Carbone L. Pain management standards in the eighth edition of the guide for the care and use of laboratory animals. J Am Assoc Lab Anim Sci 2012;51(3):322–8 JAALAS.
[26] Liu X, Liu Z, Chen J, Zhu L, Zhang H, Quan X, et al. Pigment epithelium-derived factor increases native collateral blood flow to improve cardiac function and induce ventricular remodeling after acute myocardial infarction. J Am Heart Assoc 2019;8(22):e013323.
[27] Arsic N, Zentilin L, Zacchigna S, Santoro D, Stanta G, Salvi A, et al. Induction of functional neovascularization by combined VEGF and angiopoietin-1 gene transfer using AAV vectors. Molecular Therapy 2003;7(4):450–9.
[28] Liu X, Dong H, Huang B, Miao H, Xu Z, Yuan Y, et al. Native coronary collateral microcirculation reserve in rat hearts. J Am Heart Assoc 2019;8(5):e011220.
[29] McAvoy T, Nairn AC. Serine/threonine protein phosphatase assays. Curr Protoc Mol Biol 2010 Chapter 18:Unit18.
[30] Csortos C, Czikora I, Bogatcheva NV, Adyshev DM, Poirier C, Olah G, et al. TIMAP is a positive regulator of pulmonary endothelial barrier function. Am J Physiol Lung Cell Mol Physiol 2008;295(3):L440–50.
[31] Huang P, Wang B, Wang X, Xing M, Guo Z, Xu L. HEK293 cells exposed to microcystin-LR show reduced protein phosphatase 2A activity and more stable cytoskeletal structure when overexpressing alpha4 protein. Environ Toxicol 2017;32(1):255–64.
[32] Cohen PT. Protein phosphatase 1–targeted in many directions. J Cell Sci 2002;115(2):241–56 Pt.
[33] Gavard J, Gutkind JS. VEGF controls endothelial-cell permeability by promoting the beta-arrestin-dependent endocytosis of VE-cadherin. Nat. Cell Biol. 2006;8(11):1223–34.
[34] Asano Y, Takashima S, Asakura M, Shintani Y, Liao Y, Minamino T, et al. Lamr1 functional retroposon causes right ventricular dysplasia in mice. Nat Genet 2004;36(2):123–30.
[35] Shi Y. Serine/threonine phosphatases: mechanism through structure. Cell 2009;139(3):468–84.
[36] Qi XM, Wang F, Mortensen M, Wertz R, Chen G. Targeting an oncogenic kinase/phosphatase signaling network for cancer therapy. Acta Pharm Sin B 2018;8(4):511–7.
[37] Samatar AA, Poulikakos PI. Targeting RAS-ERK signalling in cancer: promises and challenges. Nat Rev Drug Discov 2014;13(12):928–42.
[38] Adyshev DM, Kolosova IA, Verin AD. Potential protein partners for the human TIMAP revealed by bacterial two-hybrid screening. Mol Biol Rep 2006;33(2):83–9.
[39] Li L, Kozlowski K, Wegner B, Rashid T, Yeung T, Holmes C, et al. Phosphorylation of TIMAP by glycogen synthase kinase-3beta activates its associated protein phosphatase 1. J Biol Chem 2007;282(35):25960–9.
[40] Czikora I, Kim KM, Kasa A, Becsi B, Verin AD, Gergely P, et al. Characterization of the effect of TIMAP phosphorylation on its interaction with protein phosphatase 1. Biochimie 2011;93(7):1139–45.